Dual Color Emissions of $Sr_{2-x}Ca_xP_2O_7$: Eu^{2+}, Mn^{2+} for near UV Excitation

Jinying Yu, Zhendong Hao, Xia Zhang, Yongshi Luo, Xiaojun Wang and Jiahua Zhang

J. Electrochem. Soc. 2012, Volume 159, Issue 3, Pages F56-F61.
doi: 10.1149/2.054203jes

Journal of The Electrochemical Society, **159** (3) F56-F61 (2012)
0013-4651/2012/159(3)/F56/6/$28.00 © The Electrochemical Society

Dual Color Emissions of $Sr_{2-x}Ca_xP_2O_7$: Eu^{2+}, Mn^{2+} for near UV Excitation

Jinying Yu,[a,b] Zhendong Hao,[a,z] Xia Zhang,[a] Yongshi Luo,[a] Xiaojun Wang,[c] and Jiahua Zhang[a,*,z]

[a]*Key Laboratory of Excited State Processes, Changchun Institute of Optics, Fine Mechanics and Physics, Chinese Academy of Sciences, Changchun 130033, China*
[b]*Graduate School of Chinese Academy of Sciences, Beijing 100039, China*
[c]*Department of Physics, Georgia Southern University, Statesboro, Georgia 30460, USA*

Eu^{2+}, Mn^{2+} singly and co-doped $Sr_{2-x}Ca_xP_2O_7$ phosphors (x = 0–2) are prepared by solid state reaction. Crystal phase evolution is studied as a function of Ca^{2+} content based on the experimental measurements of X-ray diffraction, photoluminescence and fluorescence decay. The x dependent emission band shapes and peak positions for both Eu^{2+} and Mn^{2+} are discussed in terms of the crystal phase types and crystal field strength in relation with Ca^{2+} substitution for Sr^{2+}. An effective energy transfer from blue emitting Eu^{2+} to orange emitting Mn^{2+} is observed in all compositions beneficial to dual color emissions. The widest emission band and intense orange emission are found in $Sr_{1.25}Ca_{0.75}P_2O_7$: Eu^{2+}, Mn^{2+}, exhibiting promising use in white light generation using near UV LEDs.
 [DOI: 10.1149/2.054203jes]

Manuscript submitted September 1, 2011; revised manuscript received December 1, 2011. Published January 6, 2012.

Since the development of GaN based blue and near ultraviolet (UV) light emitting diodes (LEDs) at the end of last century, the solid state lighting sources based on white LEDs fabricated using blue (∼460 nm) and/or near UV (∼400 nm) LED chips coated with phosphors have been widely studied.[1–8] The white LEDs employing near UV LED chips with tricolor phosphors have the advantage of less shift of color point against forward current because the white light is completely phosphor converted not like the combination of blue LED with the yellow emitting YAG: Ce^{3+} phosphor.[1]

The requirement of high color rendering index need highly efficient orange or red phosphors for white LEDs. However, there are very few inorganic red or orange phosphors with environmental stability and nontoxicity for near UV based white LEDs. It is known that Mn^{2+} ion is the most prevalent red-emitting center for luminescence. Owing to forbidden transition within $3d^5$ configuration of Mn^{2+}, the Mn^{2+} singly doped material generally exhibits weak optical absorption and in turn weak luminescence. Fortunately, co-doping of Eu^{2+} as a sensitizer can produce energy transfer from Eu^{2+} to Mn^{2+} and generate strong Mn^{2+} emission in red due to dipole allowed $4f^7 - 4f^6 5d$ transition of Eu^{2+}. Some Eu^{2+}, Mn^{2+} co-doped phosphors for near UV LED applications were reported, such as $Ba_3MgSi_2O_8$: Eu^{2+}, Mn^{2+},[2] $CaAl_2Si_2O_8$: Eu^{2+}, Mn^{2+},[3] $SrZn_2(PO_4)_2$: Eu^{2+}, Mn^{2+},[4] and $Ca_9Lu(PO_4)_7$: Eu^{2+}, Mn^{2+}.[5] Upon near UV excitation, α-$Sr_2P_2O_7$: Eu^{2+} and α-$Ca_2P_2O_7$: Eu^{2+} strongly emit at 420 nm and 416 nm, respectively. Moreover, Eu^{2+}, Mn^{2+} co-doped α-$Sr_2P_2O_7$ had been patented as phosphor for generation of white light when blended with other phosphors[9]. Our previous study demonstrated that α-$Ca_2P_2O_7$: Eu^{2+} allows Mn^{2+} to incorporate into its matrix to generate a strong additional band in orange originated from Mn^{2+} through Eu^{2+}-Mn^{2+} energy transfer, resulting in dual color (blue and orange) emissions for near UV LED chip based white LEDs.[10]

Some works have been done to modify the pyrophosphate phosphors by introducing Ca^{2+} into α-$Sr_2P_2O_7$. Woo Jung Park explored $Sr_{1.5}Ca_{0.5}P_2O_7$: Eu^{2+}, Mn^{2+} phosphor[11] with a blue emission band of Eu^{2+} peaking at 425 nm and a orange one of Mn^{2+} at 614 nm. Similarly, Tae-Gon Kim discussed $Sr_{1.8}Ca_{0.2}P_2O_7$: Eu^{2+}, Mn^{2+} phosphor[12] with a blue band at 430 nm and a orange one at 610 nm. In this paper, we present systematic investigation on crystal phase formation and correlated photoluminescent properties in Eu^{2+}, Mn^{2+} doubly doped $Sr_{2-x}Ca_xP_2O_7$ with Ca^{2+} content x in a wide range from 0 to 2.

* Electrochemical Society Active Member.
z E-mail: haozhendong0451@yahoo.cn; zhangjh@ciomp.ac.cn

Experimental

Powder samples are prepared by high temperature solid-state reaction. The mixtures of analytical grade $SrHPO_4$, $CaHPO_4$, $(NH_4)_2HPO_4$, $MnCO_3$ and Eu_2O_3 are employed as starting materials in molar ratio of $Sr_{2-x}Ca_xP_2O_7$:4% Eu^{2+}, 12% Mn^{2+} with various x (x = 0, 0.25, 0.5, 0.75, 1, 1.25, 1.5, 1.75, 2). After a good mixing in an agate mortar, the mixtures are sintered at 1200°C for 4 h in CO reducing atmosphere. The structure of sintered samples is identified by X-ray powder diffractometer (XRD) (Rigaku D/M AX-2500V). The measurements of photoluminescence (PL) and photoluminescence excitation (PLE) spectra are performed by a Hitachi F4500 fluorescent spectrometer. In fluorescence lifetime measurements, the third harmonic (355 nm) of a Nd doped yttrium aluminum garnet laser (Spectra-Physics, GCR130) is used as an excitation source, and the signals are detected with a Tektronix digital oscilloscope (TDS 3052).

Results and Discussion

Figure 1 shows the PL (λ_{ex} = 330 nm) and PLE spectra (λ_{em} = peak positions) for Eu^{2+} singly doped $Sr_{2-x}Ca_xP_2O_7$: 4% Eu^{2+} with x in the range of 0 – 2. The PL bands are attributed to the transition from the lowest lying $4f^6 5d$ state to the $4f^7$ ground state of Eu^{2+}. The PLE spectra cover the UV and near UV spectral region that are assigned to the $4f^7$ - $4f^6 5d$ transition of Eu^{2+}. The PL band peaks at 420 nm for x = 0 and 416 nm for x = 2. It is observed that both the shape and position of the PL band correlate to x. This correlation is resulted from variation of crystal field environments around Eu^{2+} due to Ca^{2+} substitution for Sr^{2+} that will be discussed later.

The PL (λ_{ex} = 403 nm) and PLE (λ_{em} = peak positions) spectra of Mn^{2+} singly doped $Sr_{2-x}Ca_xP_2O_7$: 12% Mn^{2+} (x = 0 – 2) are shown in Figure 2. Each PL spectrum shows an emission band of Mn^{2+}, which is originated from the spin-forbidden $^4T_1$ - $^6A_1$ transition of Mn^{2+}. The PL band peaks at 572 nm for x = 0 and performs a redshift from 572 nm to 603 nm with increasing x up to 1.75. Further increasing x to 2, this band however shifts to the blue and finally peaks at 597 nm. Each PLE spectrum shows a dominant band at around 406 nm, that is ascribed to $^6A_1$ (^6S) - [$^4A_1$ (^4G), ^4E (^4G)] forbidden transition of Mn^{2+}.

The comparison of the PL spectrum of $Sr_{2-x}Ca_xP_2O_7$: 4% Eu^{2+} with the PLE spectrum of $Sr_{2-x}Ca_xP_2O_7$: 12%Mn^{2+} for each x reveals a significant spectral overlap, indicating the possibility of energy transfer from Eu^{2+} to Mn^{2+} in $Sr_{2-x}Ca_xP_2O_7$ phosphors. Figure 3 shows the PL (λ_{ex} = 330 nm) and PLE (λ_{em} = peak positions) spectra of Eu^{2+} and Mn^{2+} codoped $Sr_{2-x}Ca_xP_2O_7$: 4%

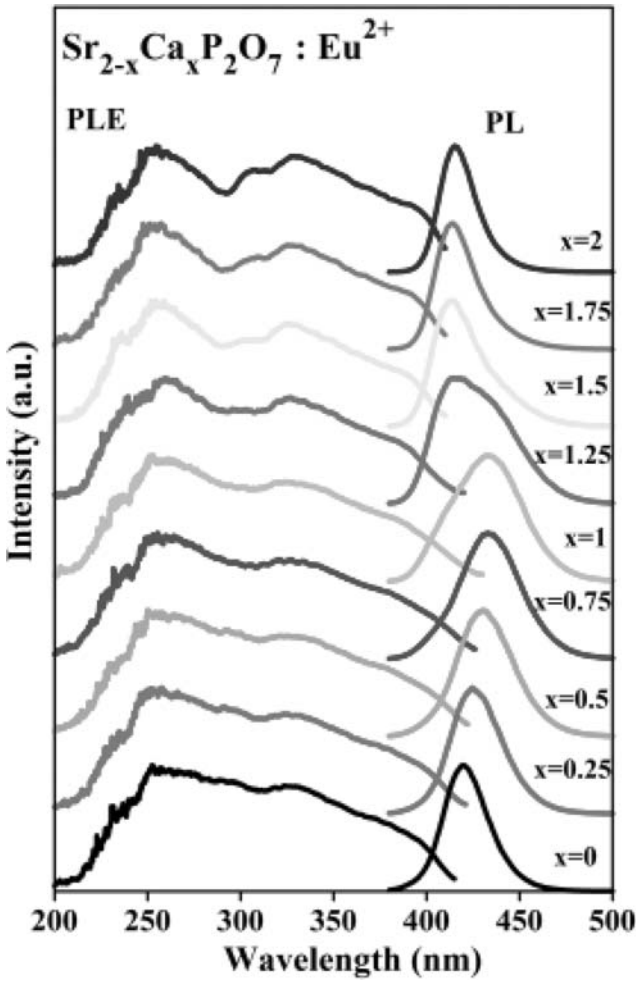

Figure 1. PL (λ_{ex} = 330 nm) and PLE (λ_{em} = peak positions) spectra of $Sr_{2-x}Ca_xP_2O_7$: 4% Eu^{2+} (x = 0, 0.25, 0.5, 0.75, 1, 1.25, 1.5, 1.75, 2).

Eu^{2+}, 12% Mn^{2+} (x = 0–2). As expected, the emission spectra exhibit not only a blue band of Eu^{2+} but also an orange band of Mn^{2+} as only Eu^{2+} is excited at 330 nm. It is also clearly demonstrated that the PLE spectrum for each x for the orange band of Mn^{2+} is no longer identical to that in Mn^{2+} singly doped material, but is consistent with that of the blue band of Eu^{2+}, indicating the performance of effective energy transfer from Eu^{2+} to Mn^{2+} in the doubly doped material. The PLE spectra imply that the doubly doped phosphors are dual color emissive and suitable for near-UV LED excitation.

The XRD patterns of $Sr_{2-x}Ca_xP_2O_7$: 4% Eu^{2+}, 12% Mn^{2+} (x = 0–2) are shown in Figure 4a. One can observe the evolution of crystalline structure from α-$Sr_2P_2O_7$ type phase with orthorhombic form (JCPDS 24–1011) to α-$Ca_2P_2O_7$ type phase with monoclinic form (JCPDS card 09-0345) with increasing Ca^{2+} composition x from 0 to 2. The monotonic shift to higher diffraction angles of the main XRD peaks with increasing x is attributed to the increasing replacement of Sr^{2+} with ionic radius of 1.12 Å by small Ca^{2+} (0.99 Å). The formation of the minor by-product $Ca_3(PO_4)_2$ phase (JCPDS 70-2065, *) appears for x >1. The impact of the minor by-product on our investigated photoluminescence properties can be excluded because the emission band (480 nm)[13] of $Ca_3(PO_4)_2$: Eu^{2+} is not detected in PL spectra. The fine XRD patterns for 2θ degree within 25.0° and 28.5° are exhibited in Figure 4b. It shows that the XRD pattern for each x within 0–0.75 is identical to the α-$Sr_2P_2O_7$ type phase except of angle shift. This indicates that $Sr_{2-x}Ca_xP_2O_7$: 4% Eu^{2+}, 12% Mn^{2+} forms a complete solid solution in α-$Sr_2P_2O_7$ type phase for x ≤ 0.75. As further increasing x to 1, an additional peak(▽) appears,

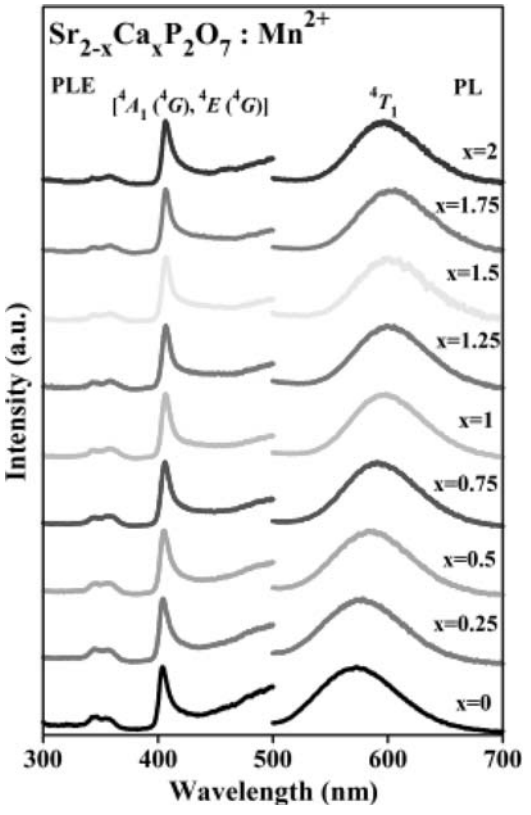

Figure 2. PL (λ_{ex} = 403 nm) and PLE (λ_{em} = peak positions) spectra of $Sr_{2-x}Ca_xP_2O_7$: 12% Mn^{2+} (x = 0, 0.25, 0.5, 0.75, 1, 1.25, 1.5, 1.75, 2).

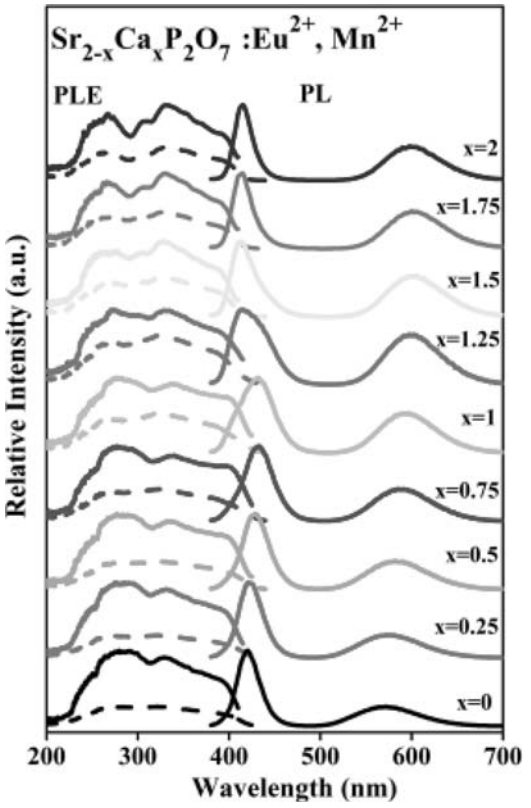

Figure 3. PL (λ_{ex} = 330 nm) and PLE (solid: Eu^{2+}, dash: Mn^{2+}, λ_{em} = peak positions) spectra of $Sr_{2-x}Ca_xP_2O_7$: 4% Eu^{2+}, 12% Mn^{2+} (x = 0–2) phosphors.

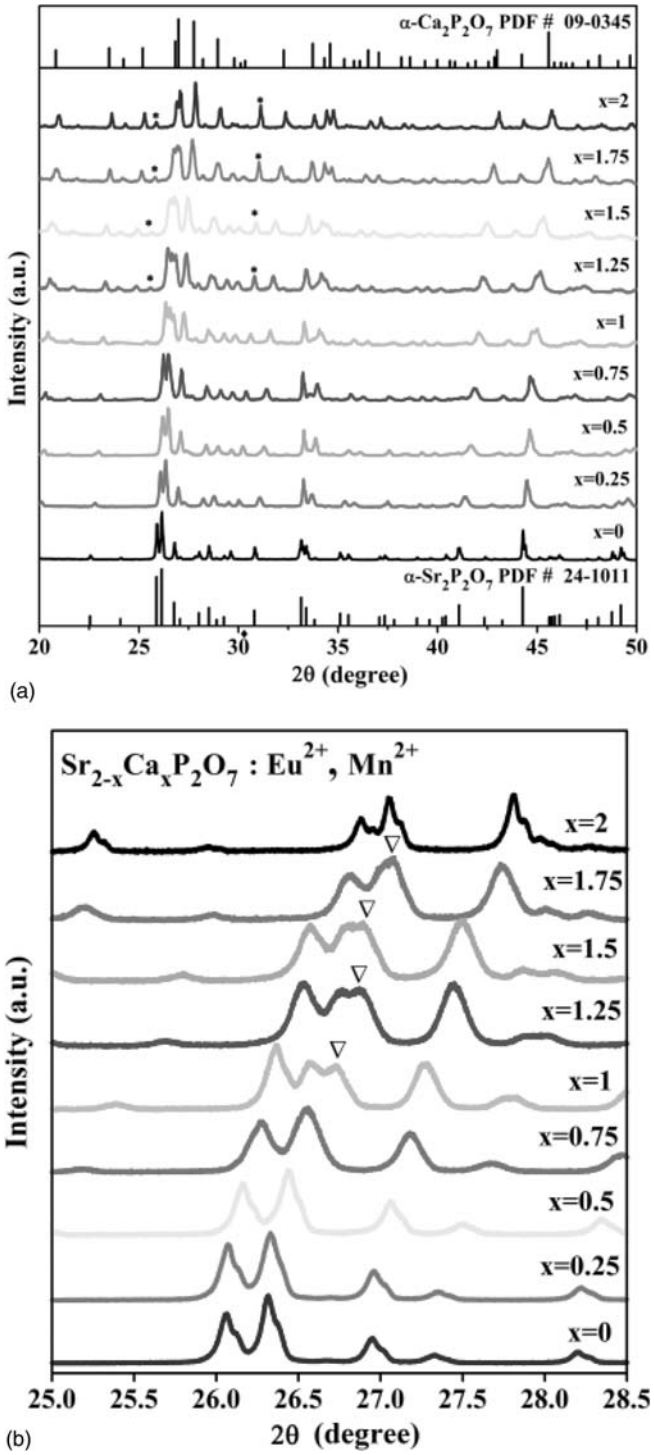

Figure 4. (a) XRD patterns of $Sr_{2-x}Ca_xP_2O_7$: 4% Eu^{2+}, 12% Mn^{2+} (x = 0–2) phosphors and the standard α-$Sr_2P_2O_7$ (NO.24–10 11), α-$Ca_2P_2O_7$(NO.09-0345). ⋆: Diffraction peak of $Ca_3(PO_4)_2$ phase. (b) Fine XRD patterns for 2θ degree within 25.0° and 28.5° of $Sr_{2-x}Ca_xP_2O_7$: 4% Eu^{2+}, 12% Mn^{2+} (x = 0–2) phosphors.

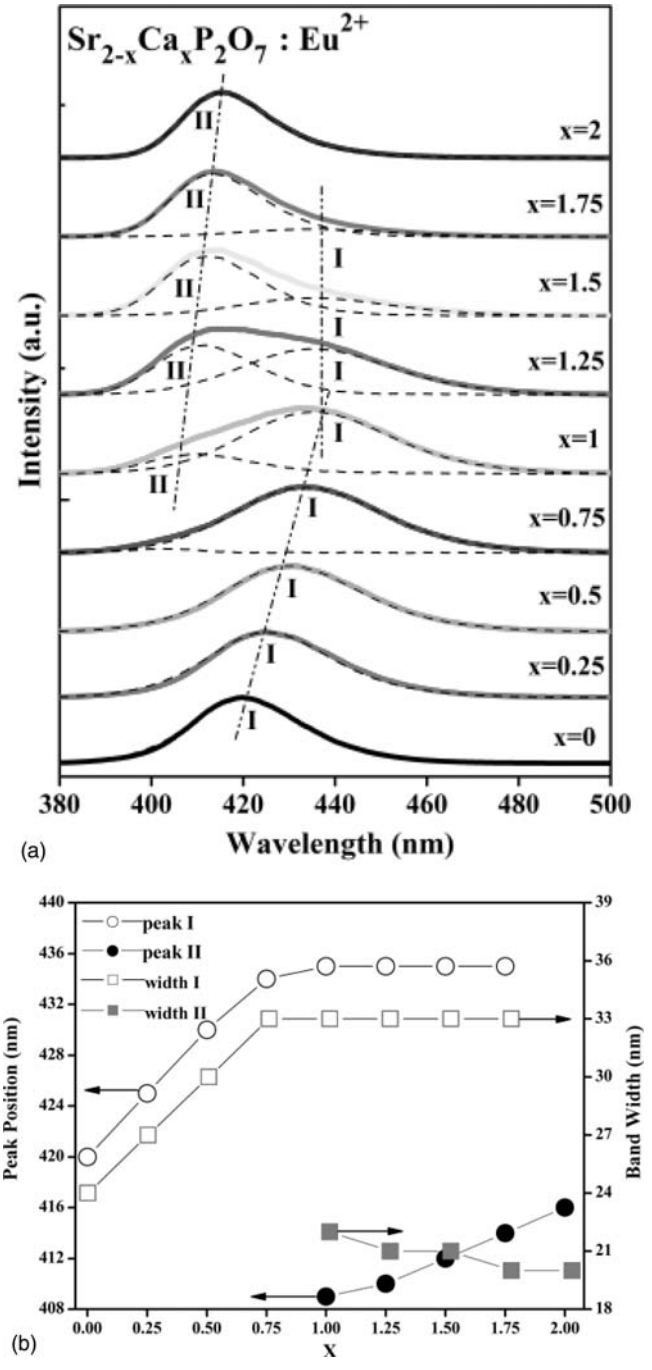

Figure 5. (a) PL (λ_{ex} = 330 nm) spectra of $Sr_{2-x}Ca_xP_2O_7$: 4% Eu^{2+} (x = 0 – 2) phosphors and the fitting results (dash line). (b) Peak positions and band widths of Eu^{2+}(I) band and Eu^{2+}(II) band.

implying the formation of α-$Ca_2P_2O_7$ type phase, that is confirmed by the correlated luminescent properties in the following parts.

The PL bands of Eu^{2+} in $Sr_{2-x}Ca_xP_2O_7$ strongly correlate to x, as shown in detail in Figure 5a. Each PL spectrum for x within 1 to 1.75 can be fitted by two Gaussian bands, in which the lower energy band is named as Eu^{2+}(I) band and the higher energy one is Eu^{2+}(II) band, as shown in Figure 5a. The fitting results are summarized in Figure 5b. For Eu^{2+}(I), the peak position shifts from 420 nm to 435 nm followed by band broadening from 24 nm to 33 nm with increasing x from 0 to 1. Further increasing x beyond 1, both the position and bandwidth of Eu^{2+}(I) band keep unchanged. The redshift of Eu^{2+}(I) band is ascribed to the enhancement of the crystal field strength due to Ca^{2+} partial substitution for Sr^{2+} in α-$Sr_2P_2O_7$ type phase. The band broadening is attributed to inhomogeneous broadening due to random substitution. The unchanged position and width of Eu^{2+}(I) band for x > 1 are explained as follows. In view of the continuous shift of the XRD peak to higher angle, the Ca^{2+} substitution for Sr^{2+} may continuously take place with increasing x. The observation of Eu^{2+}(II) band followed

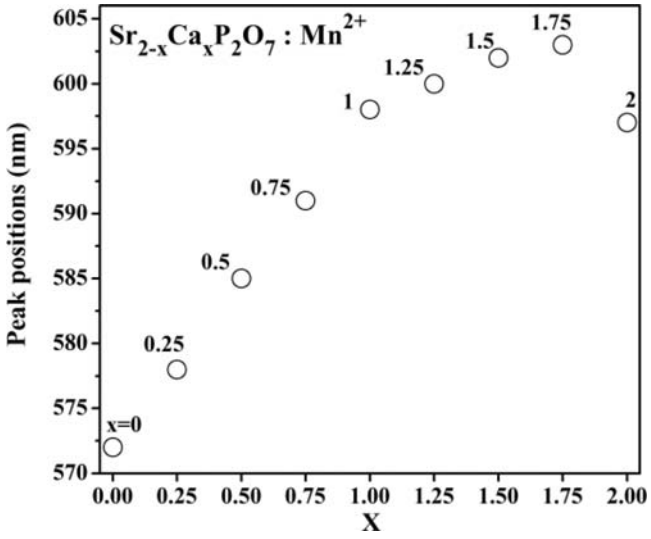

Figure 6. Peak positions of Mn^{2+} in $Sr_{2-x}Ca_xP_2O_7$ (x = 0 – 2) phosphors.

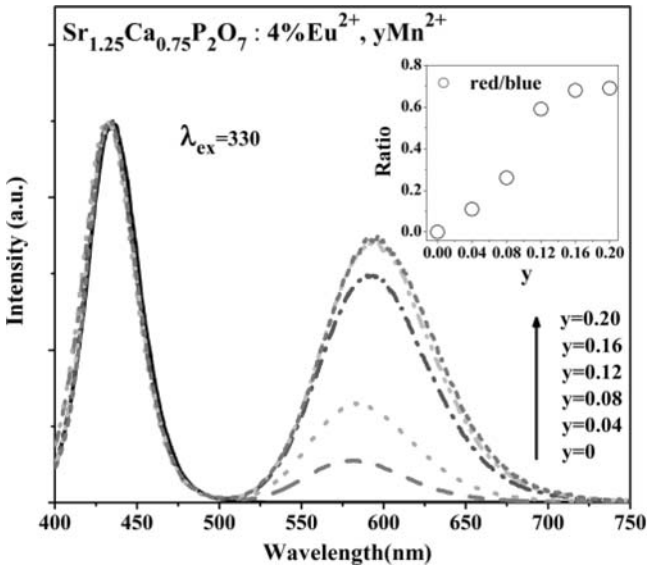

Figure 7. PL spectra (λ_{ex} = 330 nm) with normalized Eu^{2+} peak intensities for $Sr_{1.25}Ca_{0.75}P_2O_7$: 4%Eu^{2+}, yMn^{2+} (y = 0, 0.04, 0.08, 0.12, 0.16, 0.2) phosphors. Inset: relative emission intensity ratios of orange to blue on Mn^{2+} content y.

by appearance of the new XRD peak($\triangledown$) indicates the formation of α-$Ca_2P_2O_7$ type phase for x ≥ 1. The cease of redshift of Eu^{2+}(I) band for x > 1 is speculated as the result of formation of deformed α-$Sr_2P_2O_7$ type phase which perhaps tends to the α-$Ca_2P_2O_7$ type phase that forces the emission band of Eu^{2+} toward the high energy side and in turn compensates the redshift of Eu^{2+}(I) band due to Ca^{2+} substitution for Sr^{2+}. Meanwhile, the environmental disorder of α-$Sr_2P_2O_7$ type phase reaches the maximum at x = 1 and keeps unchanged for x ≥ 1.

For Eu^{2+}(II) band, it appears at x = 1 and subsequently shifts to the red side followed by band narrowing on increasing x. As a result, $Sr_{2-x}Ca_xP_2O_7$: Eu^{2+} starts to form α-$Ca_2P_2O_7$ type phase for x ≥ 1. With increasing x, the crystal field strength is enhanced due to Ca^{2+} substitution for Sr^{2+} which therefore leads to an redshift of Eu^{2+}(II) band. While the environmental disorder decreases with increasing of Ca^{2+} substitution for Sr^{2+} in α-$Ca_2P_2O_7$ type phase until pure α-$Ca_2P_2O_7$ forms for x = 2.

On the analysis above, the crystal phase of $Sr_{2-x}Ca_xP_2O_7$: Eu^{2+}, Mn^{2+} is dependent on x. For 0 ≤ x ≤ 0.75, the materials keep pure α-$Sr_2P_2O_7$ type phase. For 1 ≤ x<2, the system is speculated consisting of two mixed phases of deformed α-$Sr_2P_2O_7$ type phase and pure α-$Ca_2P_2O_7$ type phase. For x = 2, the phosphor is pure α-$Ca_2P_2O_7$ type phase. The x correlated crystal phases and environments in turn also change the position of Mn^{2+} emission band. The enhanced crystal field strength also forces Mn^{2+} band to shift toward red on increasing x up to 1.75, as shown in Figure 6. However, this band shifts back to blue as x reaches 2. This behavior can be explained as follows. The $Ca_2P_2O_7$ phase is the predominate phase in $Sr_{2-x}Ca_xP_2O_7$: 4% Eu^{2+} for x within 1.75 to 2. It was confirmed by Park et al. and Jang et al. that the octahedral symmetry around the Sr^{2+} ions is lowered as Sr^{2+} sites are substituted by Ba^{2+} in Sr_3SiO_5 : Eu^{2+}.[14,15] Accordingly, the octahedral symmetry around Ca^{2+} in $Sr_{2-x}Ca_xP_2O_7$: 4% Eu^{2+} for x = 2 ($Ca_2P_2O_7$: 4% Eu^{2+}) is higher than the case of Ca^{2+} are partially substituted by Sr^{2+} for x = 1.75 ($Sr_{0.25}Ca_{1.75}P_2O_7$: 4% Eu^{2+}), that means the crystal field symmetry around Ca^{2+} is highered as for increasing x from 1.75 to 2. The highered crystal field symmetry therefore reduces the crystal field splitting of Mn^{2+} energy levels as Mn^{2+} occupying Ca^{2+} sites and in turn results in the blue shift of the emission band of Mn^{2+} for increasing x from 1.75 to 2. As for increasing x from 0 to 1.75, the enhanced crystal field strength ascribed to the increasing substitution of Sr^{2+} by Ca^{2+} dominates the Mn^{2+} emission band and forces Mn^{2+} band to shift toward red on increasing x up to 1.75.

The phosphor $Sr_{1.25}Ca_{0.75}P_2O_7$: Eu^{2+}, Mn^{2+} (x = 0.75) crystallizing in single α-$Sr_2P_2O_7$ type phase is selected for further investigation because of the widest spectra distribution in blue and red region which benefits to near UV LED based white LEDs. Furthermore, we experimentally observed that $Sr_{1.25}Ca_{0.75}$ P_2O_7 : Eu^{2+}, Mn^{2+} exhibits the largest emission intensity ratios of orange to blue in the $Sr_{2-x}Ca_x$ P_2O_7 : Eu^{2+}, Mn^{2+} for fixed Eu^{2+} and Mn^{2+} concentrations. This means $Sr_{1.25}Ca_{0.75}P_2O_7$: Eu^{2+}, Mn^{2+} has advantage to generate warm white light with high color rendering.

Figure 7 shows the PL spectra (λ_{ex} = 330 nm) for $Sr_{1.25}Ca_{0.75}P_2O_7$: 4%Eu^{2+}, yMn^{2+} (y = 0, 0.04, 0.08, 0.12, 0.16, 0.2) of which the emission intensities of Eu^{2+} are normalized. The emission peak wavelength of Mn^{2+} shifts from 581 nm to 595 nm with the increase of Mn^{2+} content y in the range of 0.04–0.20. The redshift benefits to UV LED applications, whereas the emission peak of Eu^{2+} does not change. The emission intensity ratios of orange to blue are illustrated in the inset. As the concentration of Mn^{2+} increases, the emission intensity ratios increase monotonically due to enhanced energy transfer from Eu^{2+} to Mn^{2+}. To further understand the effect of energy transfer on luminescent properties, the decay curves of Mn^{2+} fluorescence and Eu^{2+} fluorescence in $Sr_{1.25}Ca_{0.75}P_2O_7$: 4%Eu^{2+}, yMn^{2+} are measured and plotted in Figures 8a and 8b, respectively. It is observed that the Mn^{2+} fluorescence decays exponentially and keeps an unchanged lifetime (τ_{Mn}) at around 15 ms for various Mn^{2+} concentrations. This means no concentration quenching occurs in the range of Mn^{2+} concentration of this work. However, the Eu^{2+} fluorescence decays exponentially only for low Mn^{2+} concentration with lifetime (τ_{Eu}) at around 616 ns. As increasing y, the decay of Eu^{2+} fluorescence becomes faster and more non-exponential, reflecting the characteristics of energy transfer from donors to acceptors.[16,17] The energy transfer efficiency η_T for $Eu^{2+} \rightarrow Mn^{2+}$ can be calculated using the equation,

$$\eta_T = 1 - \tau_{Eu}/\tau_{Eu,0} \quad [1]$$

where $\tau_{Eu,0}$ is the fluorescence lifetime of Eu^{2+} in $Sr_{1.25}Ca_{0.75}P_2O_7$ without codoping of Mn^{2+}. The lifetimes for Eu^{2+} are obtained by integrating the decay curves with the normalized initial intensities. The results are plotted in the inset of Fig. 8b. With increasing Mn^{2+} concentration, the energy transfer efficiency η_T increases gradually and reaches to as high as 53% for y = 0.2.

Under steady excitation, the rate equation describing the energy transfers from Eu^{2+} to Mn^{2+} can be written as follows:

$$Wn_{Eu} = n_{Mn}/\tau_{Mn} \quad [2]$$

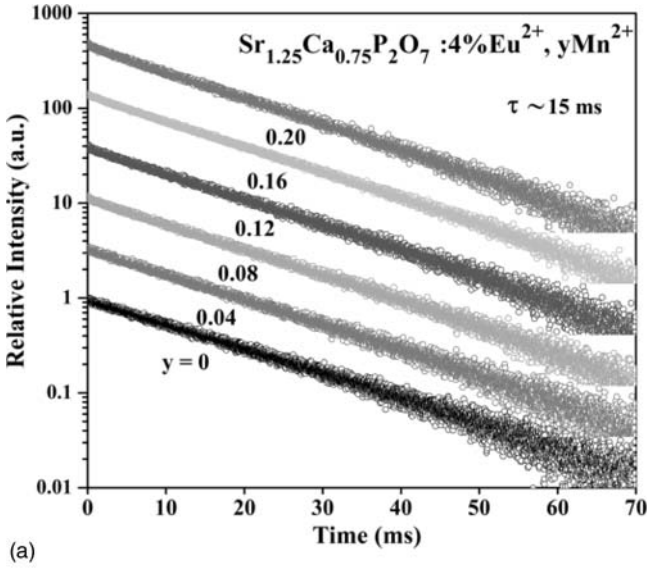

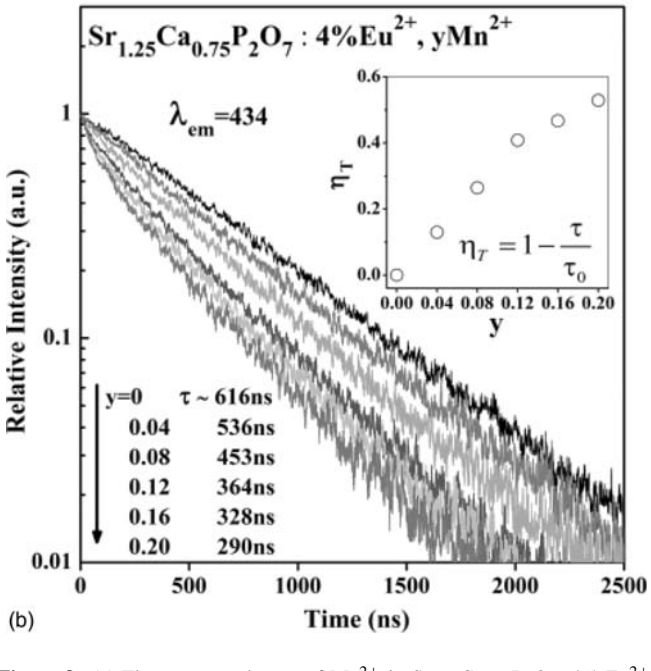

Figure 8. (a) Fluorescence decays of Mn^{2+} in $Sr_{1.25}Ca_{0.75}P_2O_7$: 4% Eu^{2+}, yMn^{2+} (y = 0, 0.04, 0.08, 0.12, 0.16, 0.2) phosphors. (b) Fluorescence decays of Eu^{2+} in $Sr_{1.25}Ca_{0.75}P_2O_7$: 4%Eu^{2+}, yMn^{2+} (y = 0, 0.04, 0.08, 0.12, 0.16, 0.2) phosphors. Inset: the dependence of the energy transfer efficiency η_T on Mn^{2+} content y in $Sr_{1.25}Ca_{0.75}P_2O_7$: 4%Eu^{2+}, yMn^{2+}.

where n_{Eu} and n_{Mn} are the population of excited Eu^{2+}, Mn^{2+} ions, respectively; $W = 1/\tau_{Eu} - 1/\tau_{Eu,0}$ is the macroscopic energy transfer rate from Eu^{2+} to Mn^{2+}.

Using Eqs. 12, the emission intensity ratio of Mn^{2+} to Eu^{2+}, *R*, is written as

$$R = \eta_T \eta_{Mn}/(1 - \eta_T) \quad [3]$$

where η_{Mn} is emission efficiency of Mn^{2+}, which is considered to be independent on y because of unchanged fluorescence lifetime of Mn^{2+} on y.

Using Eq. 3, we can get the variation tendency of the ratio R on y basing on the measured fluorescence lifetimes of Eu^{2+}. Figure 9 shows the comparison of y dependence of the ratio R calculated using Eq. 3 and obtained directly from PL spectra. From y = 0 to y = 0.16, the calculated *R* and the measured one coincide with each other very well,

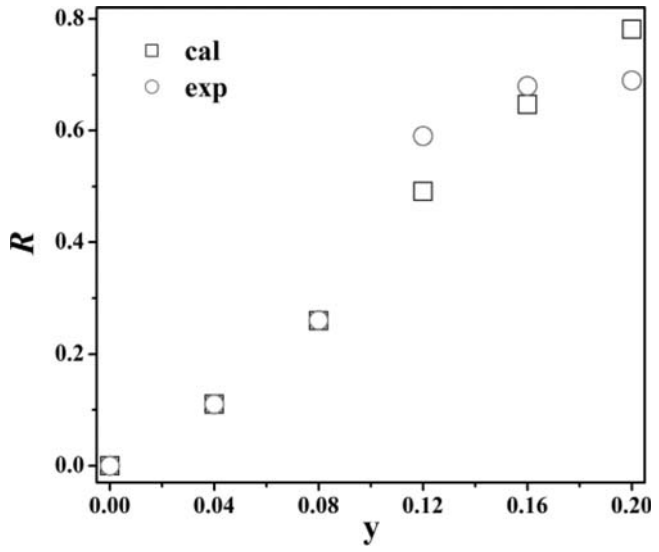

Figure 9. y dependence of emission intensity ratios of orange to blue, *R*, calculated using lifetime data and obtained directly from the spectroscopic measurements.

whereas for y = 0.2, they are dismatch. The reason for this is deducing as follows. At low Mn^{2+} concentration y (y ≤ 0.16), η_T increases with increasing Mn^{2+} concentration y due to the enhancement of energy transfer from Eu^{2+} to Mn^{2+}, η_T calculated by Eq. 1 is correct to reflect the non-radiative $Eu^{2+} \rightarrow Mn^{2+}$ energy transfer, hence the calculated *R* based on η_T and the measured *R* coincide with each other very well. However, for Mn^{2+} concentration y as high as y = 0.2, the higher dopant Mn^{2+} could introduce many defects to the matrix, the non-radiative energy transfer from Eu^{2+} to the defects is enhanced and can not be ignored. The non-exponential decay of Eu^{2+} results from both the non-radiative energy transfer from Eu^{2+} to Mn^{2+} and to the defects, the fluorescence decay of Eu^{2+} should be accelerated. It may be not appropriate to calculate the $Eu^{2+} \rightarrow Mn^{2+}$ energy transfer efficiency η_T by Eq. 1, hence the calculated *R* based on η_T should be not proper accordingly, and the additional energy transfer from Eu^{2+} to the defects should make the calculated *R* is larger than the measured one for y = 0.2.

For comparing luminescence intensities of dual color emissions phosphor and two-phosphors system, the Sr_3SiO_5: Eu^{2+} phosphor (LMS-series) is employed as the orange emission source due to its intense and similar emission (~585 nm) as Mn^{2+} doped $Sr_{1.25}Ca_{0.75}P_2O_7$. Fig. 10 shows the PL spectra (Main: λ_{ex} = 400 nm, Inset: λ_{ex} = 330 nm) of $Sr_{1.25}Ca_{0.75}P_2O_7$: Eu^{2+} (SCPOE), Sr_3SiO_5: Eu^{2+} (SSOE), $Sr_{1.25}Ca_{0.75}P_2O_7$: Eu^{2+}, Mn^{2+}(SCPOEM) and the mixtures of $Sr_{1.25}Ca_{0.75}P_2O_7$: Eu^{2+} /Sr_3SiO_5: Eu^{2+} (blends) in mass ratios of 1:1 and 1:3. Obviously, the spectra of the mixtures exhibit the emission colors of the two phosphors blends. One can observe the blue emission in the mixtures decreases drastically with increasing Sr_3SiO_5: Eu^{2+} blended, and the intensity is much lower than that in $Sr_{1.25}Ca_{0.75}P_2O_7$: Eu^{2+}, Mn^{2+} for both 400 nm and 330 nm excitation. The orange emission for the mixtures however increases with increasing Sr_3SiO_5: Eu^{2+} blended. Its integrated emission intensity is about 74% and 119% of that of $Sr_{1.25}Ca_{0.75}P_2O_7$: Eu^{2+}, Mn^{2+} phosphor for 1:1 and 1:3 mixtures, respectively, under the same 400 nm excitation which is beneficial to simulate Sr_3SiO_5: Eu^{2+}.[18] However, as for 330 nm excitation which is beneficial to simulate $Sr_{1.25}Ca_{0.75}P_2O_7$: Eu^{2+}, Mn^{2+}, the integrated orange intensity for 1:3 mixture turns to 75% of that of $Sr_{1.25}Ca_{0.75}P_2O_7$: Eu^{2+}, Mn^{2+}. The relative intensities of the whole (blue and red) spectra have not been pointed out in this work because of the incomplete blue emission for the measured spectra. The analysis above reveals the advantage of the dual color emission phosphor over the two-phosphors system for potential application to near UV-based white LEDs ascribed to the intense emission intensity.

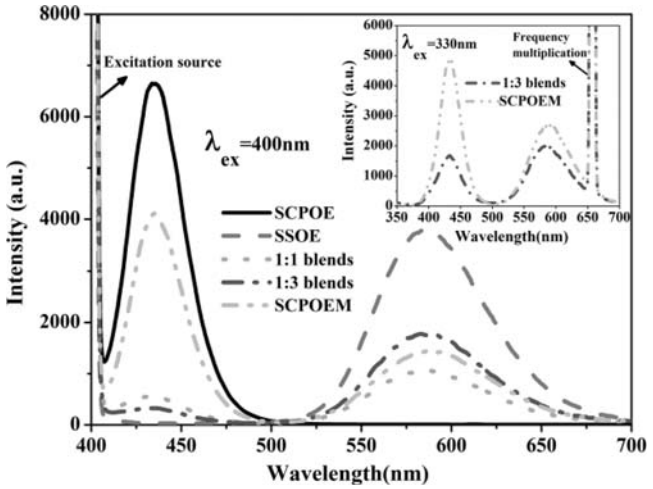

Figure 10. PL spectra (Main: λ_{ex} = 400 nm, Inset: λ_{ex} = 330 nm) of $Sr_{1.25}Ca_{0.75}P_2O_7$: Eu^{2+} (SCPOE), Sr_3SiO_5: Eu^{2+} (SSOE), $Sr_{1.25}Ca_{0.75}P_2O_7$: Eu^{2+}, Mn^{2+}(SCPOEM) and the mixtures of $Sr_{1.25}Ca_{0.75}P_2O_7$: Eu^{2+} /Sr_3SiO_5: Eu^{2+} (blends) in mass ratios of 1:1 and 1:3.

Conclusions

Eu^{2+}, Mn^{2+} singly and co-doped $Sr_{2-x}Ca_xP_2O_7$ phosphors (x = 0–2) are prepared by solid state reaction. Both the emissions of Eu^{2+} and Mn^{2+} are strongly correlated to x. Crystal phase evolution is systematically studied as a function of Ca^{2+} content based on the experimental measurements of X-ray diffraction, photoluminescence and fluorescence decay. The x dependent emission band shapes and peak positions for both Eu^{2+} and Mn^{2+} are discussed in terms of the crystal phase types and crystal field strength in relation with Ca^{2+} substitution for Sr^{2+}. The $Sr_{1.25}Ca_{0.75}P_2O_7$: Eu^{2+}, Mn^{2+} phosphor (x = 0.75) crystallizing in single α-$Sr_2P_2O_7$ type phase exhibits widest spectral distribution in blue and red region. An enhancive orange emission of Mn^{2+} is observed in $Sr_{1.25}Ca_{0.75}P_2O_7$: Eu^{2+}, Mn^{2+} upon UV excitation due to the energy transfer from Eu^{2+} to Mn^{2+}. The decay curves of Mn^{2+} fluorescence and Eu^{2+} fluorescence in $Sr_{1.25}Ca_{0.75}P_2O_7$: 4%Eu^{2+}, yMn^{2+} are measured to understand the effect of energy transfer on luminescent properties. The energy transfer efficiency can be as high as 53%, making $Sr_{1.25}Ca_{0.75}P_2O_7$: Eu^{2+}, Mn^{2+} a promising dual color (blue and orange) emitting phosphor in white light generation using UV LEDs.

Acknowledgments

This work is financially supported by the National Nature Science Foundation of China (10834006, 51172226, 10904141, 10904140), the MOST of China (2010AA03A404), the Scientific project of Jilin province (20090134, 20090524) and CAS Innovation Program.

References

1. S. Nakamura and G. Fasol, *Proc. SPIE.*, **3002**, 26 (1997).
2. J. S. Kim, P. E. Jeon, J. C. Choi, H. L. Park, S. I. Mho, and G. C. Kim, *Appl. Phys. Lett.*, **84**, 2931 (2004).
3. W. J. Yang, L. Y. Luo, and T. M. Chen, et al., *Chem. Mater.*, **17**, 3883 (2005).
4. W. J. Yang and T. M. Chen, *Appl. Phys. Lett.*, **88**, 101903 (2006).
5. N. Guo, Y. J. Huang, H. P. You, M. Yang, Y. H. Song, K. Liu, and Y. H. Zheng, *Inorg. Chem.*, **49**, 10907 (2010).
6. Y. Q. Li and A. C. A. Delsing, et al., *Chem. Mater.*, **17**, 3242 (2005).
7. C. H. Huang and T. M. Chen, *Inorg. Chem.*, **50**, 5725 (2011).
8. Vengala Rao Bandi, Yung-Tang Nien, and In-Gann Chen, *J. Appl. Phys.*, **108**, 023111 (2010).
9. A. A. Setlur, A. M. Srivastava, H. A. Comanzo, and D. D. Doxsee, US Patent **6**,685,852 B2 (2004).
10. Z. D. Hao, J. H. Zhang, X. Zhang, X. Y. Sun, Y. S. Luo, S. Z. Lu, and X. J. Wang, *Appl. Phys. Lett.*, **90**, 261113 (2007).
11. W. J. Park and Y. H. Song, *J. Electrochem. Soc.*, **156**(6), J148 (2009).
12. T. G. Kim and Y. S. Kim, *J. Electrochem. Soc.*, **156**(7), J203 (2009).
13. Costas. C. Lagos,*J. Electrochem. Soc.*, **117**(5), 1189 (1970).
14. J. K. Park, K. J. Choi, J. H. Yeon, S. J. Lee, and C. H. Kim, *Appl. Phys. Lett.*, **88**, 043511 (2006).
15. H. S. Jang, Y. H. Won, and S. Vaidyanathan, et al., *J. Electrochem. Soc.*, **156**(6), J138 (2009).
16. M. M. Broer, D. L. Huber, W. M. Yen and W. K. Zwicker, *Phys. Rev. Lett.*, **49**, 394 (1982).
17. M. M. Broer, D. L. Huber, W. M. Yen, and W. K. Zwicker, *Phys. Rev. B.*, **29**, 2382 (1984).
18. J. K. Park, C. H. Kim, S. H. Park, H. D. Park and S. Y. Choi. *Appl. Phys. Lett.*, **84**, p. 1647 (2004).